JOURNAL OF GEOPHYSICAL RESEARCH, VOL. 99, NO. D9, PAGES 18,669–18,684, SEPTEMBER 20, 1994

Reflection of solar radiation by the Antarctic snow surface at ultraviolet, visible, and near-infrared wavelengths

Thomas C. Grenfell and Stephen G. Warren
Department of Atmospheric Sciences, University of Washington, Seattle

Peter C. Mullen[1]
Geophysics Program, University of Washington, Seattle

Abstract. The variation of snow albedo with wavelength across the solar spectrum from 0.3 μm in the ultraviolet (UV) to 2.5 μm in the near infrared (IR) was measured at Amundsen-Scott South Pole Station during the Antarctic summers of 1985-1986 and 1990-1991. Similar results were obtained at Vostok Station in summer 1990-1991. The albedo has a uniformly high value of 0.96-0.98 across the UV and visible spectrum, nearly independent of snow grain size and solar zenith angle, and this value probably applies throughout the interior of Antarctica. The albedo in the near IR is lower, dropping below 0.15 in the strong absorption bands at 1.5 and 2.0 μm; and it is quite sensitive to grain size and somewhat sensitive to zenith angle. Near-IR albedos were slightly lower at Vostok than at South Pole, but day-to-day variations in the measured grain size due to precipitation, drifting, and metamorphism were found to cause temporal variations in near-IR albedo larger than those due to any systematic geographical change from South Pole to Vostok. The spectrally averaged albedos ranged from 0.80 to 0.85 for both overcast and clear skies, in agreement with measurements by others at South Pole and elsewhere in Antarctica. Using a two-layer radiative transfer model, the albedo can be explained over the full wavelength range. Tests were made to correct for systematic errors in determining spectral albedo. Under clear skies at about 3000-m elevation the diffuse fraction of downward irradiance varied from 0.4 in the near UV to less than 0.01 in the near IR; knowledge of this fraction is required to correct the measured irradiance for the instrument's deviation from a perfect cosine-response. Furthermore, the deviation from cosine response is itself a function of wavelength. Under clear skies a significant error in apparent albedo can result if the instrument's cosine collector is not parallel to the surface; e.g., if the instrument is leveled parallel to the horizon, but the local snow surface is not horizontal. The soot content of the snow upwind of South Pole Station was only 0.3 ng/g. It was somewhat greater at Vostok Station but was still too small to affect the albedo at any wavelength. Bidirectional reflectance at 0.9-μm wavelength, measured from a 23-m tower at the end of summer after the sastrugi (snow dunes) had diminished, showed a pattern remarkably similar to the spectrally averaged pattern obtained from the Nimbus 7 satellite.

Introduction

The surface energy budget of the Antarctic ice sheet is dominated by radiation. In summer the four radiation terms (downward and upward shortwave, downward and upward longwave) are each in the range 100 to 400 Wm^{-2}, generally exceeding the sensible and latent heat fluxes by at least an order of magnitude [*Rusin*, 1961; *Schlatter*, 1972; *Carroll*, 1982]. Because radiation is the driving force of Antarctic climate, radiation measurement programs have been established at most of the Antarctic research stations. The measurements at high plateau locations represent the largest areas of the Antarctic continent and are therefore the most significant for its climate.

In those radiation studies, special attention has always been given to measurement of the snow albedo. This is because snow albedo is in general highly variable. It should actually be less variable on the Antarctic plateau than elsewhere, because the snow always remains well below freezing and metamorphism proceeds slowly; but since the Antarctic surface albedo is high, small differences in albedo can mean large differences in absorbed radiation. For Antarctic snow the reported spectrally averaged albedo in summer ranges from about 0.8 to 0.9 [*Liljequist*, 1956; *Hanson*, 1960; *Hoinkes*, 1961; *Kuhn et al.*, 1977; *Peterson*, 1978; *Carroll and Fitch*, 1981; *Yamanouchi*, 1983], implying a factor of 2 variation in absorbed shortwave radiation flux.

Climatological studies of the solar radiation budget throughout the year have been carried out at several interior stations: at Plateau Station [*Kuhn et al.*, 1977], at South Pole Station [*Carroll and Fitch*, 1981], and at Mizuho Station [*Yamanouchi*, 1983]; however, these studies consisted of measurements of the solar radiation only in one or two broad bands.

[1] Now at Shapeware Corporation Seattle, Washington.

Paper number 94JD01484.
0148-0227/94/94JD-01484$05.00

Our experiment focused instead on spectrally resolved measurements. These are needed to understand the controls on regional solar energy budgets, because in addition to the spectral dependence of the solar irradiance the atmosphere, clouds, and snow all have radiative properties that change considerably with wavelength across the solar spectrum. Spectral albedos are also needed to interpret remote sensing observations from satellites that observe in narrow bands at visible and near-IR wavelengths.

The Antarctic plateau has importance for global climate because of its large area, and it also provides an excellent site for testing theories of radiative transfer in snow. Radiative transfer models of snow [e.g., *Wiscombe and Warren*, 1980a; *Grenfell*, 1992] illustrate the dependence of albedo on the physical properties of the snow. The albedo of a homogeneous snowpack depends on the size and shape of the grains, the angular distribution of the incident radiation field, the concentration of absorbing impurities, the surface roughness, and for layers less than about 10 cm thick, on the thickness of the layer and the reflectance of the underlying surface. Spectral albedo measurements in the Arctic [*Grenfell and Maykut*, 1977; *Grenfell and Perovich*, 1984] could be explained by the models in the near-IR, where the albedo is low. At visible wavelengths, however, where the albedo is high, the measured albedo was not as high as the models predicted. *Warren and Wiscombe* [1980] concluded that the snow in the experiment of *Grenfell and Maykut* [1977] was not pure. The variation of absorption with wavelength indicated that the most likely absorptive impurity was graphitic carbon (soot). That idea was confirmed by *Grenfell et al.* [1981], who measured snow albedo in the Cascade Mountains and then analyzed the snow for its soot content, essentially validating the model's prediction for a mixture of soot in snow [*Warren*, 1982; *Chýlek et al.*, 1983].

Antarctic snow should be much cleaner than northern hemisphere snow, so it was puzzling that the only measurement of Antarctic snow albedo with good spectral resolution [*Kuhn and Siogas*, 1978] (reproduced as Figure 2.2 of *Schwerdtfeger* [1984]) also showed rather low values in the visible. These may have been due to experimental errors (M. Kuhn, personal communication, 1984), but another possible explanation, favored by *Warren and Wiscombe* [1980], was that they were made too close to the station and therefore subject to local pollution. This raised the possibility that radiation measurements made near large inland Antarctic stations might not accurately represent the surrounding plateau.

Part of the difficulty in interpreting snow albedo measurements lies in the complexities arising from vertical variations of grain size in the snowpack and rapid changes in illumination that may occur on time scales that are short compared with measurement times. In addition, surface roughness can degrade the accuracy of small-scale albedo measurements even if it does not appreciably change the true albedo. In a field of longitudinal snow dunes (sastrugi), which are prevalent in regions with strong prevailing winds, the local surfaces are not horizontal; they may even be in shadow if the sastrugi ridges are high and the Sun is low. Accurate measurements under clear sky would therefore require mounting the instrument high above the surface to obtain a representative field of view. Under cloudy skies the radiation field is diffuse, substantially reducing this sampling error. During the present experiments the sastrugi were small and widely spaced, so we were able to measure albedo over flat level surfaces between the sastrugi ridges.

South Pole Station is an ideal location for measuring the optical properties of snow. Because of its remote location, impurities in the snow are minimal, and because the air temperature rarely rises above -20°C, snow metamorphism proceeds very slowly. In addition, the solar zenith angle changes negligibly over a 24-hour period. Consequently, long intervals of stable conditions exist so that comprehensive studies of the optical properties of the snow are possible.

The objectives of our project were to determine the spectral albedo (α_λ) of snow across the solar spectrum from 0.3- to 2.5-μm wavelength and to obtain the corresponding depth profiles of density and grain radius to test the consistency between observed values and results of radiative transfer models. To select measurement sites unaffected by station pollution, we also documented the extent and degree of soot pollution in snow in the vicinity of the station [*Warren and Clarke*, 1990].

Instrumentation

The first observational program was carried out at South Pole Station (90°S) during the austral summer December 1985 to February 1986. A brief description was given by *Warren et al.* [1986]. In December 1990 and January 1991, additional data were obtained at South Pole and also at Vostok Station (78°S, 107°E).

The principal instruments used in this study were intermediate resolution spectrophotometers ($\lambda/\delta\lambda$ from 25 to 50) designed specifically for polar use. The first had three parallel optical channels allowing measurements of spectral irradiance from 0.4 to 2.5 μm and was described in detail by *Grenfell* [1981]. It was battery operated to enhance portability and to avoid the need for an on-site electrical generator. The full system, including the data acquisition system, weighed less than 15 kg, was easily transportable by a single person using a backpack or a sled, and worked well at temperatures as low as -35°C. The second instrument was a filter photometer using a GaAsP photodetector to extend the spectral range into the ultraviolet with comparable spectral resolution, tolerance to low temperatures, and directional sensitivity. It had a single optical system and was about a third the size of the visible/IR instrument. Both instruments were designed to accept a fiber optics probe and collimator to measure spectral radiance above or within the snow with a field of view of about 15°. The instruments were deployed on hand-drawn sleds to avoid contamination of the measurement sites by motor vehicles.

The radiation observations were recorded with a Polycorder 516B data logger and transferred to a personal computer for processing at the station. The Polycorder was also used to drive and monitor the wavelength setting of the instruments, which greatly speeded up the observing rate.

Snow grain size was studied using a hand lens with 10-μm resolution for initial estimates together with macrophotography to provide a quantitative record. Representative depth profiles at both South Pole and Vostok are shown in Figure 1. With the lens it was possible to determine the grain radii to an estimated accuracy of about 25 μm. Snow density was measured with a Taylor-LaChapelle snow density kit to an accuracy of about 0.01 Mg m^{-3}. We were fortunate to find that the sastrugi which were built up by wind during the winter had diminished considerably during late spring, leaving large areas of flat level surface where albedos could be measured accurately from near the surface.

Irradiance and albedo studies were carried out with the instruments mounted 1.0 to 1.5 m above the surface on tripods. Measurements were made under conditions ranging from

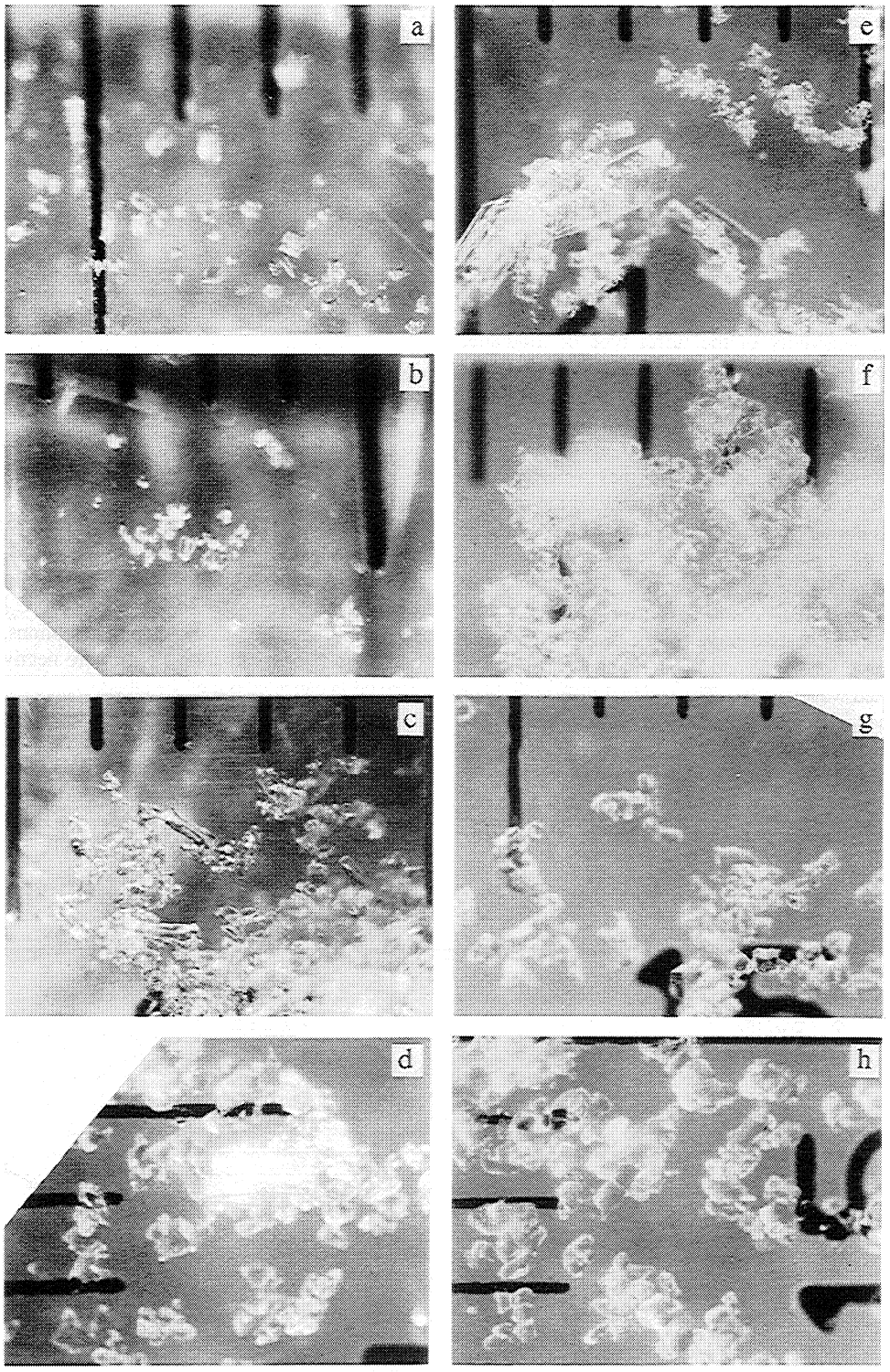

Figure 1. Partially disaggregated near-surface snow crystals at South Pole and Vostok in the summer of 1990-1991. Snow crystals were dislodged from the wall of a snowpit with a plastic ruler; the grains were then photographed as they lay on the ruler. The spacing between tick marks is 1 mm. (a) Vostok, December 29, 1990, 0-mm depth. The smallest grains in the bottom left of this photo are drift snow that fell on the ruler during photography. (b) Vostok, December 27, 1990, 1-mm depth. (c) Vostok, December 21, 1990, 4-mm depth. (d) Vostok, December 30, 1990, 20-mm depth. (e) South Pole, January 10, 1991, 0-to 5-mm depth. An example of rare surface frost. (f) South Pole, January 10, 1991, 15-mm depth. (g) South Pole, January 10, 1991,40-mm depth. (h) South Pole, January 10, 1991, 100-mm depth.

uniform overcast with the solar disk completely obscured to direct sunlight. Under clear conditions the diffuse incident spectral irradiance was recorded along with the total values to separate the direct and diffuse components of the incident radiation field for the purpose of data reduction. A silicon photodiode reference photometer was deployed at each site to record temporal variations of incident irradiance at 0.65 μm during each measurement. This made it possible to determine when the incident radiation was sufficiently stable, and in favorable cases it was possible to adjust for the variations during data reduction.

Calibration for Irradiance

The directional sensitivity of the turret type of irradiance collectors mounted on the instruments [*Grenfell*, 1981] was measured on site using a quartz halogen lamp. A series of light baffles was used to prevent stray light scattered from the walls of the hut from influencing the results. Deviations from an ideal cosine law were wavelength dependent, but they were less than about 15% at angles from 0° to 72°, which included the range of solar zenith angles during the experiment. Under clear skies the contribution from the direct solar beam was corrected using the fractional deviation of the measured response, $S(\theta)$, from a true cosine response, $\varepsilon_\lambda = [S_\lambda(\theta) - \cos\theta]/\cos\theta$, for a range of solar zenith angles. A representative curve for the departure from an ideal cosine response for the Si and PbS1 channels is shown in Figure 2 for selected wavelengths. The residual diffuse incident radiation and the reflected radiation were assumed to be isotropic; nevertheless both of these also required the application of a correction factor, C_λ, chosen such that

$$\int_0^{\pi/2} I_{\lambda,\mathrm{diff}} \cos\theta \sin\theta \, d\theta = C_\lambda \int_0^{\pi/2} I_{\lambda,\mathrm{diff}} S_\lambda(\theta) \sin\theta \, d\theta \qquad (1)$$

so that

$$F_\lambda^{\mathrm{diffuse}}(\mathrm{true}) = C_\lambda F_\lambda^{\mathrm{diffuse}}(\mathrm{observed}).$$

Introducing the definition $\mu = \cos\theta$ and assuming that $I_{\lambda,\mathrm{diff}}$ is isotropic, we can express the correction as

$$C_\lambda = 0.5 / \left\{ \int_0^1 [1 + \varepsilon_\lambda(\mu)] \, \mu \, d\mu \right\} \qquad (2)$$

and the corresponding spectral albedo is given by

$$\alpha_\lambda = \frac{F_\lambda^{\uparrow}(\mathrm{true})}{F_\lambda^{\downarrow}(\mathrm{true})} = \frac{F_\lambda^{\uparrow}(\mathrm{true})}{F_\lambda^{\downarrow}(\mathrm{diffuse,true}) + F_\lambda^{\downarrow}(\mathrm{direct,true})}$$

so

$$\alpha_\lambda = \frac{C_\lambda F_\lambda^{\uparrow}(\mathrm{obs})}{C_\lambda F_\lambda^{\downarrow}(\mathrm{diffuse,obs}) + F_\lambda^{\downarrow}(\mathrm{direct,obs}) / [1 + \varepsilon_\lambda(\theta_{\mathrm{sun}})]} . \qquad (3)$$

Equation (3) is equivalent to the correction procedure used by *Seckmeyer and Bernhard* [1993]. Values of C_λ between 0.4- and 1.2-μm wavelength and the total correction to the albedo for an example of a solar zenith angle of 68°, $C_\lambda[1 + \varepsilon_\lambda(68°)]$, are shown in Figure 3. Under cloudy conditions, both the incident and the reflected radiation fields were nearly isotropic and the correction canceled out of the albedo ratio.

A correction for the shadowing of the surface by the instrument was also applied to all upwelling irradiance measurements. The correction was determined by measuring the geometric area of the shadow and computing its contribution to the upwelling radiation under overcast conditions. The shadowing correction was 1% for the visible/IR instrument and 0.5% for the UV photometer.

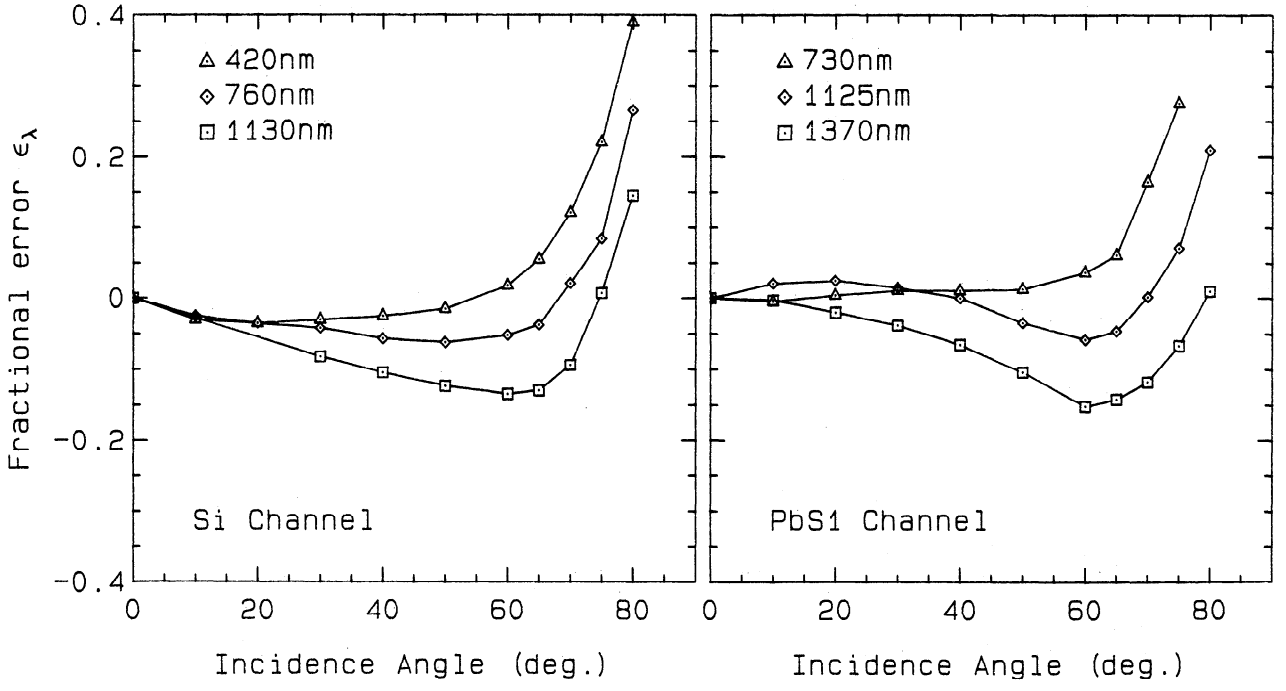

Figure 2. The departure of the turret detectors from true cosine response versus angle of an incident beam (θ) at selected wavelengths. The fractional error is defined as $\varepsilon_\lambda = [S(\theta,\lambda) - \cos\theta]/\cos\theta$, where $S(\theta,\lambda)$ is the measured directional sensitivity of the instrument.

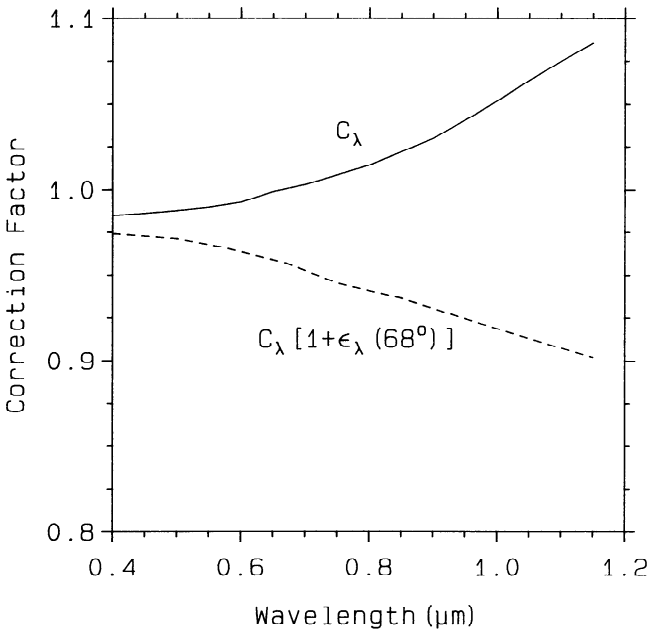

Figure 3. Albedo correction for diffuse radiation (C_λ, solid line) as well as the total correction (dashed line) versus wavelength for solar zenith angle of 68°.

Radiative Transfer Models

Our observations are compared with the results of theoretical models. The models use Mie theory for the single scattering by individual snow grains followed by a computation of multiple scattering in the snowpack. In Mie theory the scattering pattern is obtained for a single particle in isolation; however, we show below that the models agree quite well with measured spectral albedos even for closely packed snow. This is because at visible and near-infrared wavelengths the particle sizes and spaces between particles are very large compared with the wavelength of light, so one can assume incoherent scattering by the individual particles.

Since single scattering is calculated assuming spheres, we attempt to mimic the albedo of a snowpack of nonspherical particles by a model snowpack of "equivalent" spheres. When the particle size is much larger than the wavelength, which is true for snow in the visible and near infrared, *Warren* [1982] argued that a snowpack of spheres containing the same total surface area of snow grains and the same total volume of ice per square meter of the snowpack is the best way to mimic the spectral albedo of a snowpack of nonspherical particles. The spheres in the model snowpack then have the same surface-to-volume ratio as the nonspherical particles in the real snowpack, but the number of particles is greater. In many of our experiments the snow grains had been blown by the wind and were well rounded and nearly equidimensional; and it was easy to assign characteristic radii to these grains. When their shapes deviated greatly from equidimensional, the effective radius was taken to be slightly more than half the small dimension to represent the same surface-to-volume ratio [*Grenfell et al.*, 1981; *Warren*, 1982].

The reasons that one does not make large errors by assuming spherical grains were given by Craig Bohren in his review of this paper: "The orientationally averaged extinction cross section of a convex particle that is large compared with the wavelength is one-half its surface area. The absorption cross section of a large, nearly transparent particle is proportional to its volume almost independent of its shape. The closer the real part of the particle's refractive index is to 1, the more irrelevant the particle shape. The asymmetry parameter of large particles is dominated by near-forward scattering, which does not depend greatly on particle shape."

The Mie calculations used the algorithm of *Wiscombe* [1979, 1980]. They required the spectral absorption coefficient of pure ice which was measured in the laboratory by *Grenfell and Perovich* [1981] over the wavelength range 0.4 - 1.4 μm and by *Perovich and Govoni* [1991] for 0.25-0.4 μm. For λ>1.4 μm we used the values recommended by *Warren* [1984]. Subsequent to our completion of the model calculations, accurate measurements of the spectral absorption of ice from 1.4 to 2.8 μm were reported by *Kou et al.* [1993]. These are in excellent agreement with the values of *Warren* [1984] based on less accurate measurements, and our results would not change significantly if we used the data of Kou et al.

Multiple scattering in the snowpack was computed using a multilayer extension of the δ-Eddington model [*Joseph et al.*, 1976] applied by *Wiscombe and Warren* [1980a] and a four-stream discrete ordinates model [*Grenfell*, 1992]. For the present application the two models gave essentially identical results. Both models include multiple layers to represent structural variations with depth. Similar results were obtained with a two-stream model by *Bohren* [1987, his Figure 8] which used constant values of extinction efficiency, Q_{ext}, and asymmetry parameter, g, instead of wavelength-dependent values obtained from Mie theory. To obtain accurate albedos, it is thus not necessary to use Mie theory as long as a good approximation for the single-scattering albedo is used. We did, however, obtain slightly better agreement with the observations when we used the wavelength-dependent values of Q_{ext} and g from Mie theory.

In the present study, the snow grain size was chosen to be monodisperse with a different value for each model layer. For pure snow at a wavelength of 0.5 μm the downward irradiance was reduced to 1/e of its surface value at a depth of $z \approx 10$ cm suggesting that a total profile depth of about 30 cm should be sufficient to determine the spectral albedo to within 1%. Grain radii used in the model were within 25 μm of the measured values. Specific model calculations are presented below in conjunction with the corresponding observed spectra.

Albedo Observations

Spectral Albedo for Diffuse Illumination

Typical spectral albedo measurements under cloudy skies where the solar disk was completely obscured are shown in Figure 4. The primary features of α_λ are values that approach unity in the visible and ultraviolet with a gentle maximum near 0.5 μm and a slight decrease toward the near-ultraviolet wavelengths. In the infrared the α_λ drops rapidly toward longer wavelengths showing individual absorption features corresponding to the molecular absorption bands of ice [*Grenfell and Perovich*, 1981; *Kou et al.*, 1993]. This gives secondary maxima at wavelengths of about 1.1, 1.35, 1.8, and 2.25 μm. The set of observations presented in Figure 4 is an average of three scans for typical clean snow conditions taken on January 23, 1986. The corresponding grain size profile is given in Table 1.

Also shown in Figure 4 is the theoretical albedo curve for a single-layer model with a snow grain radius of $r_{int} = 100$ μm. Agreement is excellent for 0.3 to 0.9 μm, but the model

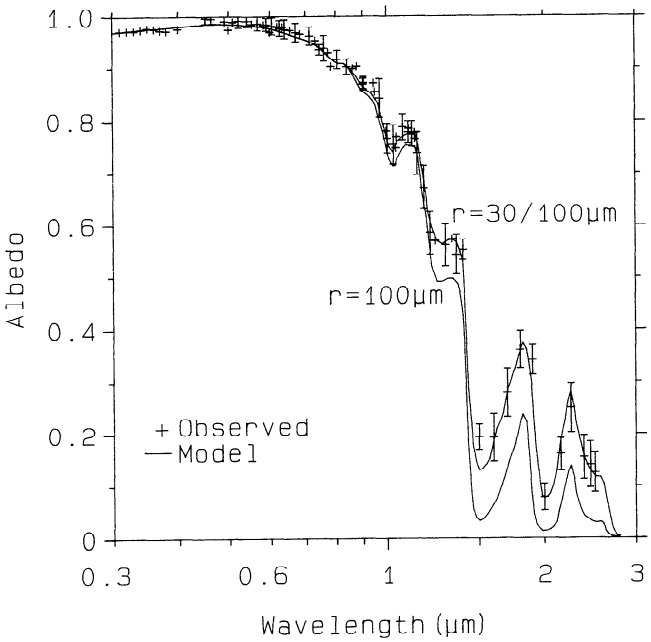

Figure 4. The observed spectral albedo for diffuse incident radiation versus wavelength for January 23, 1986, near South Pole Station [$\langle\alpha\rangle$ = 0.83]. The error bars show the standard deviation of three scans. Where they are not shown, the standard deviation is smaller than the height of the symbol. The solid lines are model results for a homogeneous layer with a grain radius of 100 μm [$\langle\alpha\rangle$ = 0.81] and for a two-layer model with a 0.25-mm thick layer of 30-μm grains over a thick layer of 100-μm grains [$\langle\alpha\rangle$ = 0.83]. NOAA's average albedo for this day was $\langle\alpha\rangle$ = 0.839.

predictions are too low at longer wavelengths. Reducing the grain radius to 50 μm causes the model prediction to be too high for λ<1.4 μm but too low for λ>1.4 μm (Figure 1 of *Warren et al.* [1986]), indicating that a vertically homogeneous snowpack cannot explain the observations. With the addition of a surface layer of thickness h = 0.25 mm and grain size r_{surf} = 30 μm, the model matched the observations throughout the entire spectral range. This illustrates the sensitivity of the near-IR albedo to snow grain size in the uppermost surface layers. For λ>1.4 μm the absorption coefficient of ice is so large that only the uppermost layer of grains can contribute significantly to the scattering. For example, in a snowpack of density 0.4 Mg m^{-3} and grain radius 100 μm, *Brandt and Warren* [1993] found that the penetration depth for photons varies from 240 mm at a wavelength of 0.47 μm to as little as 0.4 mm at 2.0 μm.

By going to a two-layer model, we are introducing two additional parameters (h and r_{surf}). There is a variety of combinations of (h, r_{surf}, r_{int}) that can cause the model to produce a good match with the observed spectral albedo within the constraints of our data; we have shown one example that is both plausible and simple. Unfortunately, in 1986 we did not recognize the potential importance of grain size variation within the top millimeter of the snowpack, so our photographs of the "surface" grains actually contain snow from the top 5 mm. At a low-elevation Antarctic site, however, *Stephenson* [1967] did find that grain radius increased in the top 7 mm from 50 μm to 160 μm. A model with smaller grains at the surface is plausible for two reasons. (1) It is well known that as snow ages the surface-to-volume ratio decreases (and thus the effective grain size increases) due to "destructive metamorphism" [*LaChapelle*, 1969] which occurs most rapidly in the first few days after the snowfall. (2) In the Antarctic, even aged snow can have significantly smaller grains at the surface because of the prevalence of wind drifting. Snow grains suspended in the drifting layer shrink by sublimation. Furthermore, as wind-drifted snow settles when the wind speed diminishes, the smallest suspended grains would be expected to fall out last, resulting in a sorting of the grains by size in the topmost layers. Smaller grains have a larger surface-to-volume ratio and therefore favor scattering over absorption. This is consistent with the observation of *Liljequist* [1956] that the spectrally averaged albedo increased after windstorms. At Vostok we photographed snow grains with average radii of 10 to 15 μm in snow drifting along the surface (the smallest grains shown in Figure 1a).

Alternatively, such small surface grains might not be required by the model to match the observations if it were to take into account the nonsphericity of the snow grains. Calculations by *Takano and Liou* [1989] have shown that deviations from spherical shape cause enhanced side scattering at the expense of forward scattering, which decreases the asymmetry factor and increases the albedo. Most of their published results were for broad wavelength bands; however, they presented monochromatic results for two wavelengths which showed that the decrease in the asymmetry parameter was greater at 0.55 μm than at 2.2 μm for all particle sizes (their Table 3).

To investigate this effect in snow, we extended to smaller asymmetry parameters the calculations shown in Figure 19 of *Wiscombe and Warren* [1980a]. Using these results, we found that the changes in asymmetry parameter needed to match the observed albedo with a single homogeneous layer were negligible at 0.55 μm and much larger at 2.2 μm, where a decrease in g of about 0.3 was needed. Since this is opposite to the result of *Takano and Liou*'s [1989] model, we favor the two-layer interpretation; and the two-layer model with a thin layer of 30-μm grains overlying a thick layer of 100-μm grains will be used as a reference in several model calculations below.

In a remote-sensing study, *Carlson et al.* [1992] attempted to exploit the sensitivity of near-infrared albedo to grain size. They used a ratio of reflectances at 1.7 μm and 1.5 μm from the Galileo flyby of Antarctica on December 8, 1990, to map the distribution of surface grain size, obtaining radii ranging from about 50 to 200 μm. If those estimates are accurate, our value of 30 μm may be smaller than the average for the Antarctic continent. The Galileo measurements are discussed further below.

Visible and Ultraviolet Albedo

The visible and ultraviolet portion of Figure 4 is shown with greater resolution in Figure 5. The observational curve is slightly bowed with a maximum between about 0.45 and 0.5 μm. Compared with this are the model results of Figure 4. The agreement is within 0.012 at all wavelengths. We have also included the South Pole results of *Kuhn and Siogas* [1978], the only previous measurements of spectral albedo on the Antarctic plateau. These values are much lower than either the present data or the model calculations. They imply a spectrally averaged albedo of 0.76, lower than other measurements in the interior of Antarctica. The major difference is in the visible, while in the near infrared their results are reasonably consistent with our

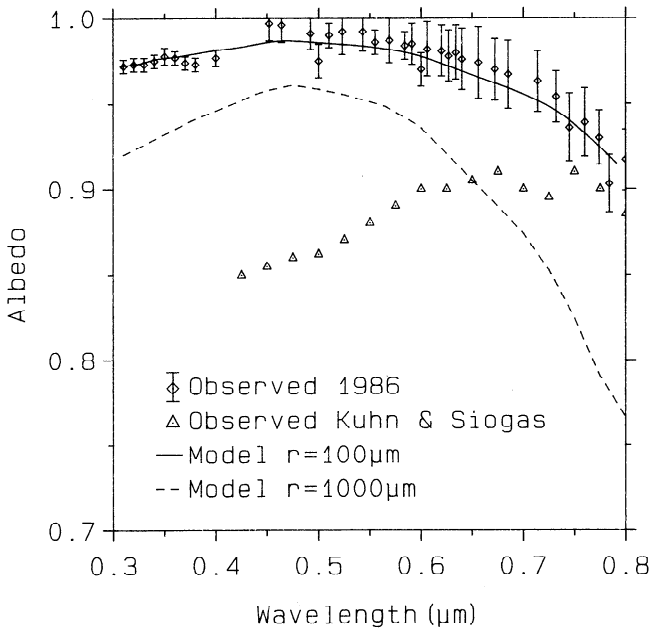

Figure 5. Ultraviolet and visible spectral albedos from Figure 4 compared with the data of *Kuhn and Siogas* [1978] and with model results for two different grain sizes.

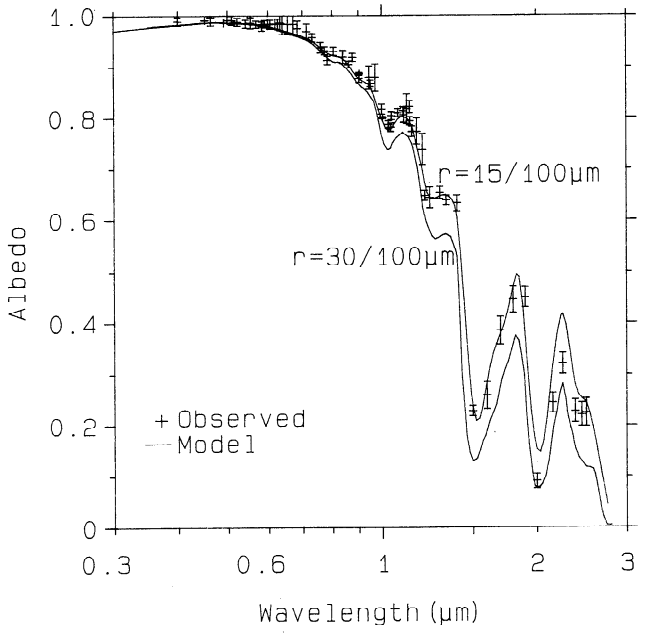

Figure 6. The spectral albedo for diffuse incident radiation versus wavelength for a layer of new snow on wind-packed snow (January 2, 1986) [$\langle\alpha\rangle = 0.85$]. The solid lines are model results for two-layer models with a 0.25-mm layer of 30-μm [$\langle\alpha\rangle = 0.83$] and 15-μm grains [$\langle\alpha\rangle = 0.85$] as indicated. The bottom curve here is the same as the top curve in Figure 4. NOAA's average albedo for this day was $\langle\alpha\rangle = 0.87$.

models [*Warren and Wiscombe*, 1980, Figure 1] and observations.

The low visible albedo of *Kuhn and Siogas* [1978] cannot be explained by any realistic grain size. As shown in Figure 5, their measured albedos are lower than would be expected even for a grain radius of 1000 μm, typical of old melting snow. *Warren and Wiscombe* [1980] explained this discrepancy by proposing that the snow measured by Kuhn and Siogas contained 750 ng of soot per gram of snow (ng/g). The soot survey of *Warren and Clarke* [1990], however, found no more than 3 ng/g of soot even downwind of the station where the concentration was greatest. We therefore favor other explanations such as neglect of a large shadowing correction or other experimental errors (M. Kuhn, personal communication, 1984).

Albedo After New Snow Deposition

Observations made directly after a new snowfall on January 2, 1986 (Figure 6), show significantly higher albedos. The difference relative to Figure 4 ranges from 0.005 near 0.7 μm to as much as 0.04 in the near infrared. In this case, the only difference in snowpack structure was that the ice grain radius estimated visually in the upper few millimeters was smaller (20 to 40 μm). The corresponding theoretical curve is shown as a solid line in Figure 6, and the observed grain size profile is listed in Table 1. The addition of a thin fine-grained layer with r = 15 μm matched the near infrared quite well and produced almost no change in the visible. Unfortunately, our photographs from that day were not in focus. To obtain an independent estimate for the size of newly fallen snow grains before undergoing any destructive metamorphism, we use the measurements by *Kikuchi and Hogan* [1979] of a-axis and c-axis lengths in summertime snow crystals (primarily hexagonal columns) at South Pole Station to compute the size of equivalent spheres by the method described above. The resulting frequency distribution of radii can be characterized by its "effective radius" (surface-area-weighted mean radius [*Hansen and Travis*, 1974]), which is 17.5 μm. Thus we think that a surface grain radius of 15 μm is not unreasonable in the model.

Clear Sky Albedos

Spectral albedo under clear skies is shown in Figure 7a for solar zenith angles of 55°, 68°, and 72°. Because these observations were made several weeks apart, the grain-size profiles were somewhat different. To isolate the effect of zenith angle alone we also show model calculations for the above zenith angles in Figure 7b. In general, the albedos are greater for larger solar zenith angle. The differences are quite small for high albedos, primarily in the visible, and also for very low values, in parts of the infrared, and they are largest for intermediate values, as will be further illustrated in Figure 11 below. The observed increase of albedo with zenith angle is also predicted by the models. The reason that the albedo is higher for larger zenith angles is that a photon, on average,

Table 1. Mean Snow Grain Radius Versus Depth Below Surface at South Pole in 1986 for Snow Whose Albedo is Shown in Figures 4-6

Depth, mm	January 23	January 2, New Snowfall
0-5	50 μm	25 μm
5-50	50-150	50-150
50-100	100-150	100-150
100-200	100-250	100-250
200-300	150-200	150-200
300-400	150-250	150-250

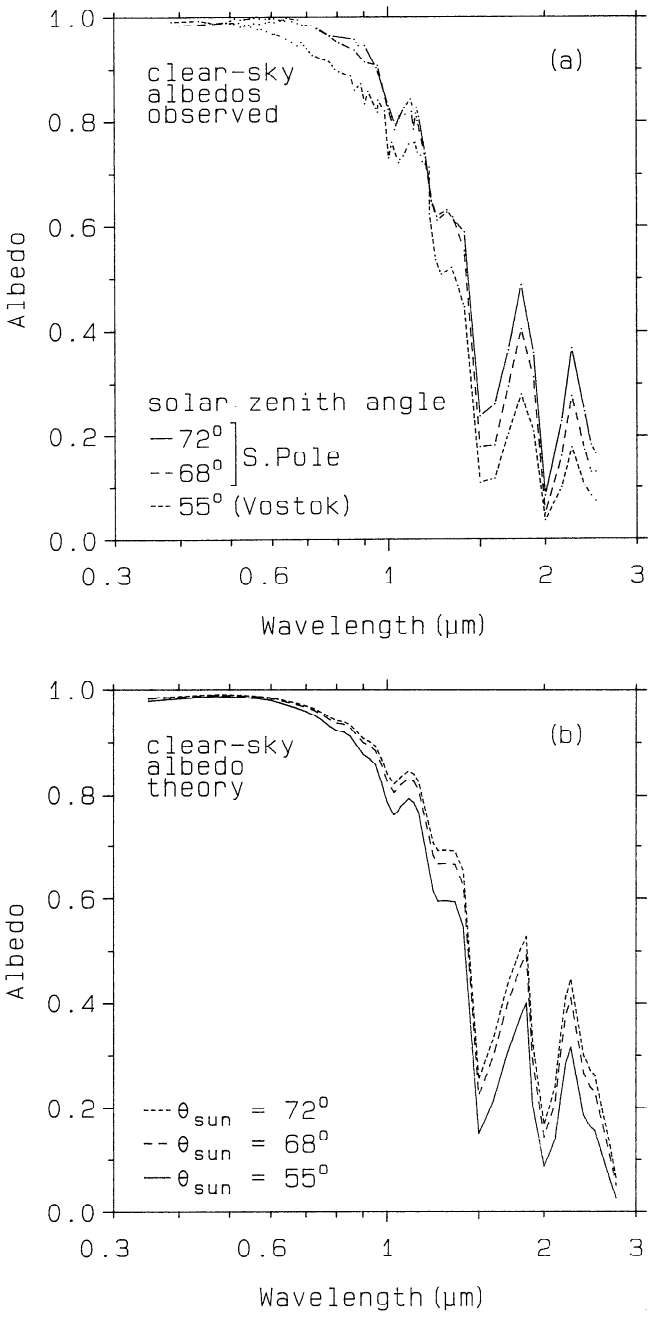

Figure 7. (a) Observed spectral albedos for clear sky illumination versus wavelength for solar zenith angles of 55° [$\langle\alpha\rangle$ = 0.80], 68° [$\langle\alpha\rangle$ = 0.84], and 72° [$\langle\alpha\rangle$ = 0.85]. The error bars have been omitted for clarity. They are the same size as in Figure 4. (b) Model calculations of spectral albedo for clear sky illumination versus wavelength for solar zenith angles of 55° [$\langle\alpha\rangle$ = 0.83], 68° [$\langle\alpha\rangle$ = 0.85], and 72° [$\langle\alpha\rangle$ = 0.85]. The snowpack parameters are the same as those used for the top curve in Figure 4, the two-layer model.

undergoes its first scattering event closer to the surface if it enters the snow at a more nearly grazing angle. If the scattering event sends it in an upward direction, its chance of escaping the snowpack without being absorbed is greater than it would be if it were scattered from deeper in the pack.

In the near infrared the observed albedos (Figure 7a) are lower than the model albedos (Figure 7b) for all three cases.

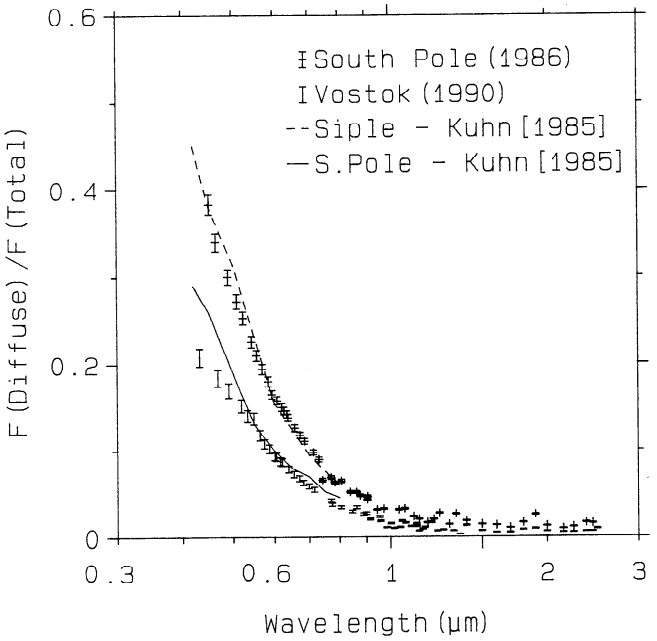

Figure 8. Observations of the ratio of diffuse to total (D/T) radiation under clear sky conditions. Results of *Kuhn* [1985] are included for reference. Station elevations are as follows: South Pole, 2835 m; Vostok, 3488 m; Siple Station, 1054 m. We apparently used a smaller shade than did Kuhn, so we measured a larger fraction of diffuse radiation.

This discrepancy could be due to surface grains being larger on clear days with greater absorption of sunlight and destructive metamorphism, or to inaccurate characterizations of the cosine collector, or it could indicate a fault in the model.

Between 0.6 and 1.0 μm, however, where the albedo should be relatively insensitive to both grain size and zenith angle, the observed albedo is higher than the model calculation at South Pole for 68° and 72° but lower than the model calculation at Vostok for 55°. We cannot explain these discrepancies; however, we note again here, as elsewhere, that albedo is more difficult to measure accurately under a clear sky than under diffuse illumination.

Diffuse Radiation From a Clear Sky

The ratios of diffuse to total incident irradiance (D/T) are shown in Figure 8. The values from South Pole decrease from about 0.40 at 0.4 μm to less than 0.01 beyond 0.9 μm. The values of D/T are greater at South Pole mainly due to the larger zenith angles. At both locations, however, the D/T ratios are about twice what would be expected from pure Rayleigh scattering by a molecular atmosphere [*McCartney*, 1976, Figure 4.8]. In both 1986 and 1990 the optical depth of stratospheric aerosol was only about 0.01 [*Dutton and Christy*, 1992], so the

Table 2. Empirical Fit of Diffuse to Total Incident Irradiance on Cloud-Free Days to $D/T = B*\lambda^A$

Site	A	B	Correlation Coefficient	Solar Zenith Angle
South Pole	-3.26	0.0305	0.995	67-72°
Vostok	-3.33	0.0165	0.985	55-64°

deviation of D/T from its Rayleigh value is probably due to small atmospheric ice crystals in an apparently clear sky.

Between 0.4 and 1.0 μm the wavelength dependence of D/T fits well to a power law (Table 2). The exponent of -3.3 differs slightly from that of Rayleigh scattering (-4) due to multiple Rayleigh scattering and because some of the scattering was by particles.

Albedo of a Sloping Surface

An important potential source of error in albedo measurement under clear skies is the tilt of the surface away from horizontal. Surface slope can introduce errors in mountainous regions because of the large slope angles and at high latitudes because even small slopes cause significant error at large solar zenith angle.

For a plane surface the dominant effect is that the incident irradiance with respect to the local zenith is different from the irradiance incident with respect to the normal of the sloping surface. For the case of a small surface slope, isotropic reflected radiance, and an instrument set up with the cosine collector parallel to the horizon, the apparent albedo, $\alpha_\lambda(\text{ap})$, is given by

$$\alpha_\lambda(\text{ap}) = \alpha_\lambda(\text{true})\frac{\cos[\theta_{\text{sun}} + \theta_{\text{surf}}\cos\varphi]}{\cos\theta_{\text{sun}}}\left[1-\frac{\theta_{\text{surf}}}{2}\right], \qquad (4)$$

where θ_{sun} is the solar zenith angle, θ_{surf} is the slope of the surface in radians, and φ is the solar azimuth defined as zero when the solar azimuth is in the uphill direction from the detector. The second factor in brackets in equation (4) accounts for the projection of the incident irradiance onto the sloped surface and is the dominant effect. The third factor accounts for the slice in the downward hemisphere that would be filled with snow if the surface were level. This factor is close to unity for small slope values but gives rise to an azimuthally independent shift which amplifies slightly the asymmetry in the apparent albedos for the uphill and downhill directions (φ=0° and 180°) with respect to the flat surface albedo. At an azimuth of 90° the only effect is due to this slice. For high Sun the slope effect is modest, but at large zenith angles typical of polar latitudes, it increases rapidly.

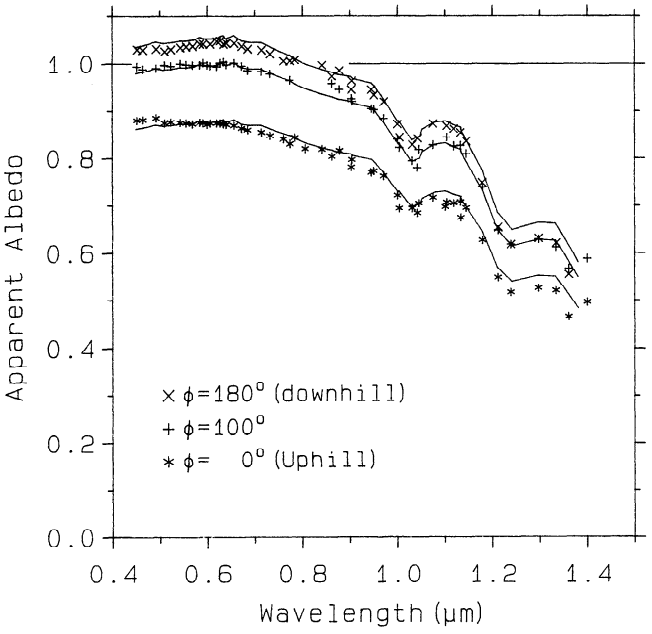

Figure 9. The effect of a surface slope of 2° on apparent spectral albedo. The observations are denoted by the points. The model curves are derived from smoothed albedo observations for a level surface, corrected for slope using equation (4).

Observations were carried out on a surface with a slope of 2° at a solar zenith angle of 70°, and the results are indicated by the individual points in Figure 9. The results from equation (4) are also included as solid lines. For α_λ(true) in equation (4) we have used a smoothed curve passed through the average of all our measurements of $\alpha_\lambda(70°)$ made over level surfaces. In the visible the apparent albedo reached a maximum value at 0.6 μm of about 1.04 for the Sun in the downhill direction and a corresponding minimum of 0.87 when the Sun was in the uphill direction. Equation (4) predicts a total variation of about 20% giving apparent albedos between $0.89\alpha_\lambda$(true) and $1.08\alpha_\lambda$(true). These predictions match the observations (Figure 9) quite well throughout the visible wavelength region.

Beyond 1.4 μm the model did not match the observations. In this case, the reflected radiance was increasingly influenced by single scattering and the assumption of nearly isotropic upwelling radiance was probably no longer a good approximation. A more thorough investigation of this phenomenon, however, is rather complex and is beyond the scope of the present work.

Effect of Soot Contamination

A comprehensive study of the near-surface soot content in and around South Pole Station [*Warren and Clarke*, 1990] showed that the concentration in our observation area was about 0.3 ng/g, which was close to the background level measured 13 km upwind of the station. The calculations of *Warren and Wiscombe* [1980, their Figure 7a and footnote 3] indicated that a uniform distribution of 15 ng/g of soot is needed to produce a 1% decrease in spectral albedo of fine-grained snow at the most sensitive wavelength (0.5 μm) if the spatial distribution of soot is assumed to be randomly located external to the snow grains. About half as much soot is needed to cause the same reduction of albedo in the case of soot particles inside the snow grains [*Chýlek et al.*, 1983; *Bohren*, 1986]. The more realistic case of soot particles on the surfaces of the grains would have an intermediate effect on albedo. In general, the soot levels appear to be a factor of 20 too low to have a measurable effect on the observations reported here. Contamination can be significant, however, if the albedo is measured too close to the station, as we observed on one occasion.

Soot Survey at Vostok

To choose a clean site for albedo measurements at Vostok Station, we measured the soot content of the snow at the locations indicated in Figure 10. To determine the impurity levels in the snow, we used the technique of *Warren and Clarke* [1990]. Samples of between 3 and 6 liters of snow were melted and run through a 0.4-μm nuclepore filter under a vacuum allowing the impurities to be deposited uniformly over the filter. The snow was melted quickly in a microwave oven and poured immediately into the filtering apparatus to minimize adherence of soot to the walls of the glass containers. The nuclepore filter collected almost all the soot. The most ever obtained on backup filters during calibration of the method was 5% (A. Clarke, personal communication, 1986). Absolute soot content was obtained by assuming a specific absorption of 9.68 $m^2\ g^{-1}$ and

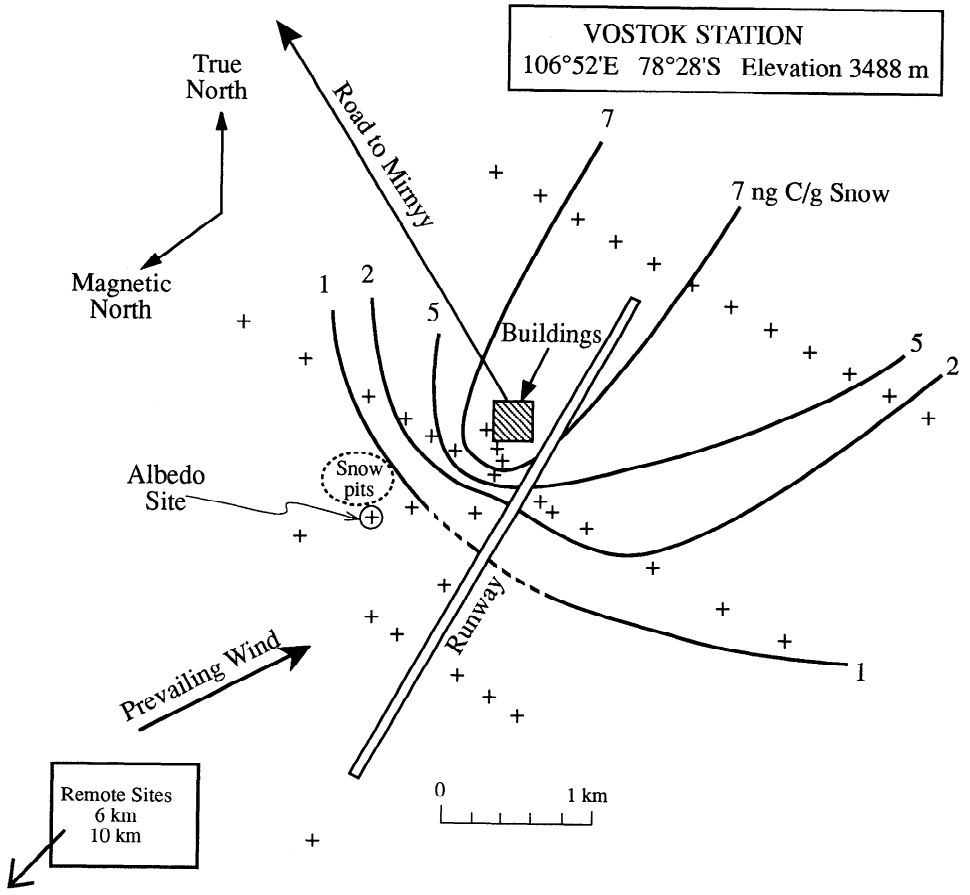

Figure 10. Diagram of contamination of the snow by soot (carbon) at Vostok Station in nanograms per gram. Sampling sites are indicated by plus signs.

measuring the transmissivity of the filters [*Clarke et al.*, 1987]. The estimated absolute uncertainty is a factor of 2-3, but relative values are more accurate. In the field the darkness of the filters was compared against a standard set provided by Antony Clarke. It was thus possible to achieve useful results on station in near real time. For the 1986 experiment at South Pole, both the filters and the frozen snow samples were brought home to the United States and processed in the laboratory to calibrate the field technique.

Contour lines of soot content based on the Vostok filter samples are shown in Figure 10. All samples used to draw the contour lines were taken from sastrugi to represent approximate upper limits to the soot content. The contour lines are only approximate because of scatter in the data. The pattern, showing a plume in the downwind direction, is similar to that at South Pole Station mapped by *Warren and Clarke* [1990], but the soot concentrations are a factor of 2-3 higher at Vostok. This also appears to be true for the soot content in the snow collected at remote sites 6 km and 10 km upwind of Vostok, intended to represent unpolluted background snow. Samples collected 13 km upwind of South Pole Station contained 0.1-0.3 ng/g. Snow from the remote site at Vostok was determined by visual examination of the filters to contain 0.6 ng/g. The ratio of soot content at Vostok and South Pole may therefore be similar to the ratio of snow accumulation rates (2-3 g cm^{-2} yr^{-1} and 8 g cm^{-2} yr^{-1}, respectively).

Figure 10 shows that the site used for snow pit studies in years past is well chosen; it is the cleanest area at that distance from the station. The site used for measurement of surface albedo at the Vostok weather station was just upwind of the buildings, and its soot content was 7 ng/g, 20 times the concentration at the NOAA albedo-monitoring site at the South Pole Clean Air Facility. Even 7 ng/g, however, can reduce the albedo only by about 0.005, too small to be detectable.

Comparative Effects of Sun Angle, Grain Size, and Soot

Model calculations shown in some of the earlier figures are combined and replotted in Figure 11 in the form of albedo differences as a result of changing one of the controlling variables, as a function of albedo of a standard snowpack. Different points on the abscissa correspond to different wavelengths. Figure 11a shows the increase in albedo as the solar zenith angle increases from 0° to 80°. There is little change at wavelengths where the albedo is close to zero (2.0 μm) or unity (in the visible). The maximum sensitivity occurs at wavelengths where the albedo is 0.2 to 0.4 (1.0 to 1.5 μm). The same is true for the sensitivity of albedo to grain size (Figure 11b), where the albedo increases as grain size decreases.

Quite different behavior, however, arises from the addition of soot (Figure 11c). Soot in small quantities is able to reduce the snow albedo significantly only at wavelengths where the albedo is high, primarily the visible. In spectral regions where the albedo is lower due to increased absorption by the ice itself, the soot contributes less to the total absorption.

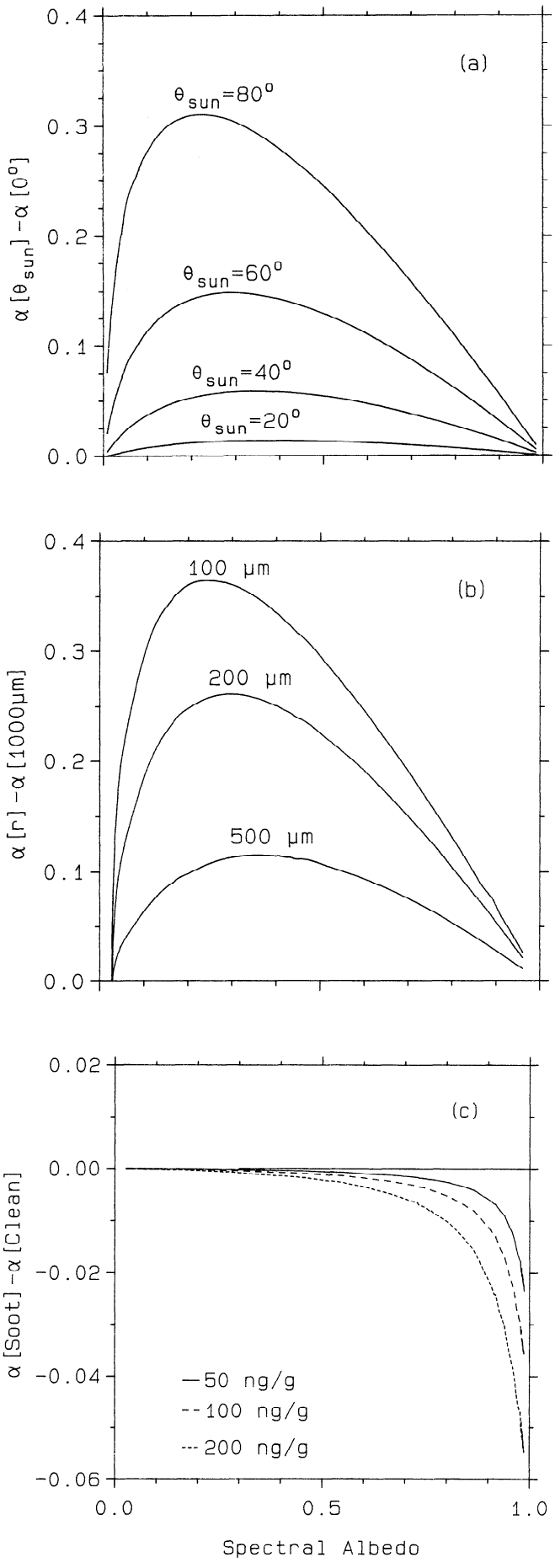

Comparison of Albedos from South Pole and Vostok

To see if there are systematic differences between the albedos observed at South Pole and Vostok, we compare the results of cloudy sky observations to eliminate differences due solely to the variations in solar zenith angles. All the results from each station were averaged, and the two average spectra are compared with each other in Figure 12a. The difference between the albedos shows no significant wavelength trend and has an average value of 0.0022 with a standard deviation of 0.03. This is negligibly different from zero at well above the 99% confidence level and is consistent with the profiles of grain size and density at the two locations (Tables 3, 4, and 5). We can therefore recommend the use of albedo measurements near either South Pole or Vostok to represent the entire East Antarctic plateau.

Carlson et al. [1992] visited Vostok Station in December 1991, one year later than we did, and found grains of 200-μm average radius, which are larger than the results given in Table 3. They concluded that their grain sizes were consistent with their inference from Galileo. However, the Galileo flyby occurred in December 1990 when we were at Vostok and measured smaller grain sizes. As a result, we feel that the algorithm for grain-size estimates from Galileo requires further validation.

Although the radiative transfer analysis shows consistency with the albedo observations and provides a general framework for computing spectral albedo, it is also useful to have purely observational estimates for averaged spectral albedos. For diffuse illumination conditions, results from different sites and stations can be compared directly. The averaged spectral albedos, including scans from 19 different sites, are enclosed by the envelope in Figure 12b. The width of the envelope is greatest in the infrared, primarily due to variations in surface grain size but also to increased noise levels at smaller incident irradiance. The regional variations among the cases we have examined appear to be small enough that for cloudy conditions the averaged values are likely to be a good representation for clean sites on the Antarctic plateau.

The average values of α_λ are listed in Table 6 together with the standard deviations. For clear sky conditions (Figure 7) the solar zenith angle should be taken into account and a single averaged α_λ curve is not appropriate.

Figure 11. Sensitivity of spectral albedo to solar zenith angle, snow grain size, and soot content plotted as functions of the spectral albedo of a reference snowpack. Different points on the abscissa correspond to different wavelengths (see Figure 4). (a) Effect of zenith angle. Plotted is the increase in albedo for the specified solar zenith angle, θ_{sun}, relative to the albedo for θ_{sun} = 0°. Grain radius is 100 μm. (b) Effect of snow grain size. Plotted is the increase in albedo for the specified grain radii relative to the albedo of a coarse-grained snowpack of r = 1000 μm; θ_{sun} = 60°. (c) Effect of soot content. Plotted is the decrease in albedo relative to a pure snowpack due to three different amounts of soot. Snow grain radius is 100 μm and θ_{sun} = 60°. The soot is assumed to be randomly distributed and external to the snow grains. These results would apply for half the stated soot amounts if the modeling had instead assumed soot particles inside the ice grains [*Chýlek et al.*, 1983].

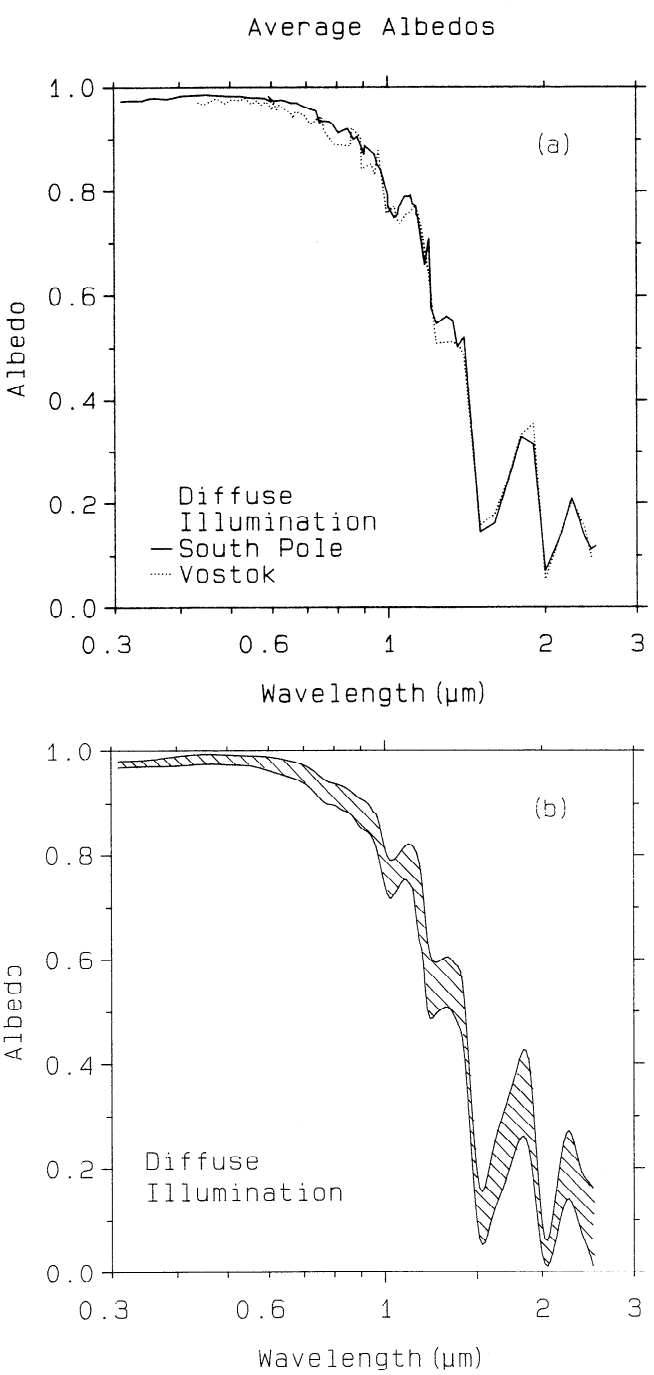

Figure 12. (a) Average spectral albedos under diffuse illumination for South Pole and Vostok. (b) The smoothed envelope of observed spectral albedo for diffuse illumination for 19 cases observed at South Pole and Vostok Stations. From the mean values of α_λ we find $\langle\alpha\rangle = 0.83$.

Spectrally Averaged Albedos

The spectrally averaged broadband albedo, $\langle\alpha\rangle$, is given by

$$\langle\alpha\rangle = \frac{\int \alpha_\lambda F_\lambda^\downarrow \, d\lambda}{\int F_\lambda^\downarrow \, d\lambda}, \qquad (5)$$

where $F_\lambda^\downarrow$ is the spectral distribution of the incident solar irradiance. Because of the uncertainty in absolute calibration of the spectrophotometer, we have used the results of an atmospheric radiation model [*Wiscombe and Warren*, 1980b; *Wiscombe et al.*, 1984] to determine $F_\lambda^\downarrow$ instead of measurements. The model spectra are for clear skies at various solar zenith angles over the Antarctic plateau and for overcast conditions of various cloud thickness. Some of these spectra were presented by *Brandt and Warren* [1993] in their Figure 1. For the solar spectrum under overcast cloud we used an average cloud thickness found by *Kuhn et al.* [1977] at Plateau Station that caused the apparent transmittance of the entire atmosphere to be 0.82. Since albedos were not measured for $\lambda > 2.5$ μm, we used model-calculated albedos for 2.5-5.0 μm. Because there is so little solar energy at these wavelengths, $\langle\alpha\rangle$ is insensitive to uncertainties in the spectral albedo used here.

Table 3. Averaged Snow Grain Radius (r) Versus Depth (z) Measured Visually in the Field

	South Pole, 1985-1986			Vostok, 1990-1991		
z, mm	r, μm	σ, μm	N	r, μm	σ, μm	N
0	73	53	9	71	64	10
5	--	--	--	83	62	9
10	58	51	5	92	68	6
20	43	51	5	83	74	6
30	--	--	--	67	35	3
50	94	71	4	185	205	6
100	98	50	5	189	162	6
150	100	--	1	--	--	--
200	180	82	5	223	186	6
300	150	71	2	296	229	6
400	300	--	1	538	407	2
500	325	233	2	500	--	1
550	250	--	1	--	--	
600	350	--	1	--	--	
650	500	--	1	--	--	

Sigma (σ) is the standard deviation of averages from N different days rather than the standard deviation in a distribution of grain sizes for a single sample.

Table 4. Profiles of Averaged Snow Grain Radius (r) Versus Depth (z) at South Pole in 1986 Together With Size Range and Number of Grains measured (N)

z, mm	r, μm	r_{min}, μm	r_{max}, μm	N
0	52	21	96	15
10	122	34	278	31
20	171	53	372	24
50	169	87	319	23
100	192	87	370	16
150	138	98	209	5
200	195	87	326	16
250	196	71	356	24
350	247	188	333	10
450	208	100	467	10
550	189	111	311	19
650	209	128	289	17

Grain sizes were measured by S.Marshall (personal communication, 1988) on our photographs.

Table 5. Profiles of Averaged Snow Density, $\langle\rho\rangle$, Versus Depth, z

South Pole					Vostok				
z(top), mm	z(bot), mm	$\langle\rho\rangle$, Mg m^{-3}	σ	N	z(top), mm	z(bot), mm	$\langle\rho\rangle$, Mg m^{-3}	σ	N
0	50	0.337	0.038	5	0	30	0.311	0.036	4
50	100	0.357	0.029	5	33	54	0.304	0.019	4
100	150	0.365	0.031	4	55	83	0.303	0.019	4
150	200	0.362	0.034	5	90	114	0.315	0.013	4
200	250	0.390	0.044	3	118	139	0.310	0.024	4
250	300	0.388	0.043	4	146	176	0.328	0.013	4
300	350	0.384	0.023	2	183	203	0.327	0.015	3
350	400	0.389	0.018	3	204	226	0.325	0.024	4
400	450	0.383	0.011	2	239	269	0.353	0.031	4
450	500	0.383	0.008	3	268	298	0.363	0.018	3
500	600	0.370	0.014	2	305	335	0.338	0.041	4
600	700	0.380	--	1	350	380	0.420	--	1
700	800	0.370	--	1	400	430	0.300	--	1
800	900	0.410	--	1					
900	1000	0.390	--	1					

Sigma is the standard deviation and N is the number of sites.

Albedos are computed for the complete solar spectrum 0.3 to 5.0 μm. We have also computed values for two broad bands that divide the spectrum into two nearly equal parts, 0.3 to 0.7 μm and 0.7 to 5.0 μm. This division at 0.7 μm is commonly used in general circulation models. The results of these calculations are given in Table 7. The absorption spectrum of clouds is very similar to that of snow, attenuating more strongly in the infrared than in the visible, because both media consist of H_2O whose shortwave absorption spectrum is nearly the same for liquid and solid phases. This causes spectrally averaged snow albedo to increase with increasing cloud opacity (Figure 5 of *Grenfell et al.* [1981], section k of *Warren* [1982], and Table 3 of *Grenfell and Perovich* [1984]).

Also shown in Table 7 are the average albedos obtained by the atmospheric monitoring station of NOAA's Climate Monitoring and Diagnostics Laboratory (CMDL) at the Clean Air Facility at South Pole Station. The average albedos for the months we were at South Pole in 1985-1986 were computed from daily average values supplied by E. Dutton (personal communication, 1994). For comparison we also show the 2-year averages for five sunlit months published by *Dutton et al.* [1989]. Their average of 0.81-0.83 is also in accord with most other measurements of snow albedo in Antarctica, e.g., those of *Yamanouchi* [1983] at Mizuho, *Kuhn et al.* [1977] at Plateau Station, and *Carroll and Fitch* [1981] at South Pole. NOAA's averages for 1985-1986 are about 3% higher than their 1986-1988 values. Our values of $\langle\alpha\rangle$ for individual overcast days in 1986 (January 2 and 23) are 1-2% lower than those measured by NOAA-CMDL, as indicated in the captions to Figures 4 and 6. This result, however, is affected by our choice of an average cloud optical thickness of $\tau = 0.6$. Clouds are probably thicker at South Pole than at Plateau Station. If τ is increased from 0.6 to 6 (the thickest cloud ever observed by Kuhn et al.), then the computed $\langle\alpha\rangle$ increases by about 0.035.

A Comment on the Effect of Sastrugi on Albedo

Wendler and Kelley [1988] measured spectrally averaged snow albedo in Terre Adélie on the slope of East Antarctica using pyranometers. They found that the surface albedo increased with cloud cover and zenith angle consistent with earlier investigations reviewed by *Warren* [1982]; however, their analysis of the effect of sastrugi on albedo in the fourth section of their paper is not correct. It consists of model calculations predicting albedo to drop below 0.2 at large solar zenith angles, in disagreement with all measurements over sastrugi fields, in particular those of *Carroll and Fitch* [1981], who reported that albedo increased monotonically with zenith angle all the way to $\theta_{sun} = 90°$. The error in Wendler and Kelley's analysis is the assumption that the albedo of shaded snow is only 0.15, whereas that of sunlit snow is 0.8. In reality the albedo, which is the probability that an incident photon interacting with the snow will reemerge above the surface, should not be significantly lower in the shadow.

To measure the albedo of a sastrugi field, one can either take many readings across the field from 1-m height, as Wendler and Kelley did, or raise the downward-looking radiometer sufficiently high above the surface (at least several meters) so that a representative field of view would be obtained which contains typical sunlit and shadowed area fractions. Their albedo measurements appear reasonable, lying in the range 0.75-0.92. We suggest that only their section "sastrugi and albedo" is based on an incorrect model. Their earlier sections, including Figures 1 through 5, appear to contain useful and valid data.

Bidirectional Reflectance of Snow

Narrow-field-of-view sensors on satellites monitoring solar radiation measure the reflected radiance in a particular direction. For climate studies of the Earth's radiation budget, the albedo is needed, which is the integral of the upward radiance over all angles, divided by the downward irradiance. To infer the albedo from a radiance measurement at only one angle, it is necessary to know the bidirectional reflectance distribution function (BRDF). The BRDF is a function of four angles: solar zenith and azimuth and satellite nadir and azimuth. For areal or temporal averages on many natural surfaces, only three angles are needed to describe the function, because only

Table 6. Averaged Spectral Albedos for Diffuse Illumination, South Pole and Vostok Data

λ, μm	α	σ	λ, μm	α	σ
0.310	0.973	0.003	0.858	0.895	0.014
0.320	0.974	0.003	0.869	0.902	0.028
0.330	0.974	0.002	0.889	0.864	0.017
0.340	0.974	0.003	0.900	0.881	0.028
0.350	0.978	0.003	0.940	0.867	0.026
0.360	0.979	0.004	0.951	0.846	0.017
0.370	0.978	0.004	0.967	0.841	0.034
0.380	0.977	0.001	0.989	0.782	0.031
0.400	0.982	0.007	0.999	0.760	0.026
0.415	0.981	0.009	1.029	0.748	0.042
0.449	0.982	0.010	1.043	0.750	0.025
0.477	0.983	0.010	1.052	0.764	0.034
0.482	0.982	0.008	1.078	0.781	0.028
0.500	0.982	0.009	1.099	0.780	0.028
0.512	0.981	0.008	1.117	0.773	0.029
0.523	0.981	0.007	1.129	0.768	0.036
0.540	0.981	0.010	1.133	0.750	0.043
0.553	0.978	0.007	1.144	0.750	0.027
0.567	0.979	0.010	1.173	0.678	0.039
0.581	0.978	0.014	1.200	0.709	0.056
0.592	0.978	0.014	1.207	0.594	0.041
0.600	0.972	0.010	1.239	0.547	0.048
0.605	0.972	0.011	1.289	0.550	0.050
0.617	0.976	0.014	1.333	0.548	0.054
0.622	0.973	0.011	1.364	0.503	0.043
0.630	0.972	0.012	1.400	0.508	0.062
0.638	0.970	0.014	1.409	0.516	0.028
0.654	0.966	0.015	1.500	0.145	0.048
0.668	0.963	0.016	1.600	0.162	0.060
0.681	0.959	0.016	1.700	0.245	0.071
0.708	0.956	0.014	1.800	0.323	0.075
0.725	0.950	0.013	1.900	0.301	0.081
0.738	0.929	0.019	2.000	0.062	0.029
0.739	0.932	0.013	2.150	0.139	0.051
0.768	0.926	0.012	2.250	0.206	0.065
0.774	0.925	0.025	2.380	0.133	0.059
0.801	0.909	0.012	2.450	0.098	0.055
0.831	0.915	0.028	2.500	0.087	0.075

the difference between the two azimuths is important, not their individual values. This assumption was made when developing empirical BRDFs from Nimbus 7 satellite data [*Taylor and Stowe*, 1984a] for use in the Earth Radiation Budget Experiment (ERBE).

In large areas of the polar regions, however, all four angles may be needed because the sastrugi are oriented parallel to a prevailing wind direction. The BRDF shows a forward peak when the solar beam is along the direction of the sastrugi but sometimes shows an enhanced backward peak when it is perpendicular. Averaging over all solar azimuths relative to the sastrugi orientation causes backscattering to be averaged together with forward scattering. The conclusion of the ERBE analysis, that snow is the most nearly isotropic of all Earth surfaces, may therefore be at least partly a result of this averaging. By altering the effective zenith angle, sastrugi can reduce the spectrally averaged albedo by an amount that varies with sastrugi orientation relative to the direction of the Sun and which averages only about 1% [*Carroll and Fitch*, 1981, Table 2]; however, sastrugi can potentially have a much greater effect on the angular pattern of reflected radiation.

Early work on the bidirectional reflectance of snow was reviewed by *Warren* [1982]. Since then *Taylor and Stowe* [1984a] obtained an average BRDF for the snow-atmosphere system from satellite observations of snow at different angles by assuming that all the snow examined at a particular zenith angle had the same albedo. The variation of BRDF with wavelength was calculated by *Li* [1982] for a flat snow surface using radiative-transfer modeling. Recent measurements at selected wavelengths for flat snow surfaces were reported by *Steffen* [1987].

The first observations of the effects of sastrugi on BRDF were made by *Kuhn* [1974, 1985] from the roof of the Clean Air Facility at the South Pole. We found South Pole Station to be an ideal location for this type of study because over the course of a day all solar azimuth angles are sampled, while the zenith angle changes are negligible. In our 1986 pilot study we measured the BRDF from the top of the 23-m tower in the clean air sector. From this vantage point, about 180° of azimuth is undisturbed snow; the other 180° contains buildings and footpaths. To complete the BRDF pattern for the unmeasurable half of the hemisphere, we used observations made 12 hours later when the Sun was in the opposite direction. The results were interpolated across the region shadowed by the tower.

We attached a fiber-optics probe from our photometer to a collimating tube mounted on a goniometer. We used only one

Table 7. Spectrally Averaged Albedo for Various Wavelength Intervals

Site/Type	0.3-5.0 μm	0.3-0.7 μm	0.7-5.0 μm
Observed			
Cloudy sky, average	0.83	0.98	0.67
Cloudy sky, upper envelope	0.85	0.99	0.71
Cloudy sky, lower envelope	0.80	0.97	0.64
Clear sky $\theta_{sun} = 72^o$ South Pole	0.85	0.99	0.72
Clear sky $\theta_{sun} = 68^o$ South Pole	0.84	0.99	0.70
Clear sky $\theta_{sun} = 55^o$ Vostok	0.80	0.98	0.63
NOAA-CMDL			
Dec. 1985*	0.83		
Jan. 1986*	0.85		
Feb. 1986*	0.87		
Oct. 1986-7†	0.83		
Nov. 1986-7†	0.82		
Dec. 1986-7†	0.81		
Jan. 1987-8†	0.82		
Feb. 1987-8†	0.83		
Modeled			
Cloudy sky			
Single layer, r = 100 μm	0.81	0.98	0.63
Two layer, r = 30 & 100 μm	0.83	0.98	0.67
Two layer, r = 15 & 100 μm	0.85	0.98	0.72
Clear sky, two layer, r = 30 and 100 μm			
$\theta_{sun} = 72^o$	0.85	0.99	0.74
$\theta_{sun} = 68^o$	0.85	0.98	0.72
$\theta_{sun} = 55^o$	0.83	0.98	0.67

NOAA-CMDL, National Oceanic and Atmospheric Administration Climate Monitoring and Diagnostics Laboratory.
* South Pole albedos from E.Dutton (personal communication, 1994).
† Two-year averages at South Pole from *Dutton et al.* [1989].

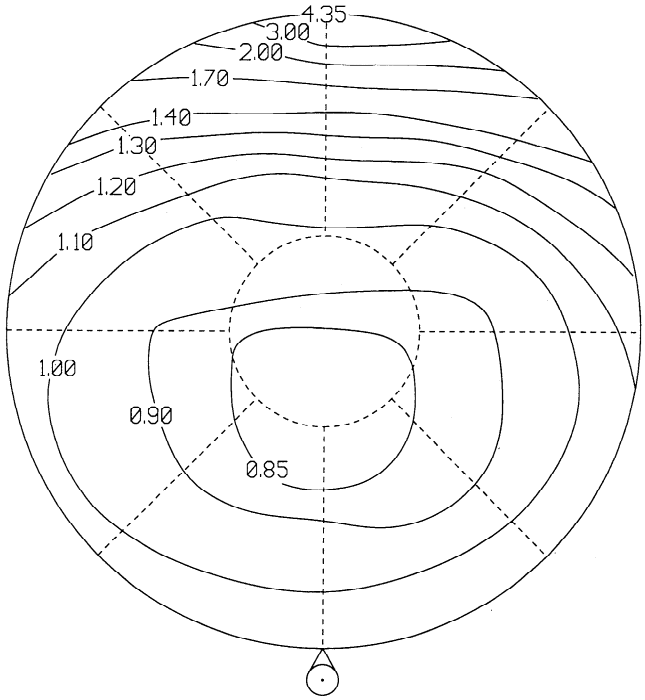

Figure 13. Bidirectional reflectance distribution function at 0.9-μm wavelength, normalized to an average value of 1.0 using equation (1) of *Taylor and Stowe* [1984b] and averaged over solar azimuth angle relative to a fixed geographical reference frame. The inside circle denotes a viewing nadir angle of 22.5° and the outside circle denotes 82.5°. The solar zenith angle was about 75°. The measurements were made at 15° intervals in both azimuth and nadir angle. The direction of the Sun is indicated by the circle and arrowhead.

wavelength (0.9 μm), where Rayleigh scattering from the sky is negligible (see Figure 8). Measurements were made once an hour with a 15° field of view at 15° intervals in viewing zenith and azimuth angles throughout the day. These measurements were made in early February 1986 on cloudless days.

All the patterns obtained were very similar, giving a forward scattering pattern similar to Taylor and Stowe's results from the top of the atmosphere. This is because the sastrugi usually diminish in prominence during the summer [*Gow*, 1965] and the surface was nearly flat in February 1986. We therefore present only the average of the patterns (Figure 13), scaled to give an average value of 1.0. The relative values are within 20% of unity over all but the forward direction, with a maximum of 4.3 in the forward direction. This pattern is remarkably consistent with the results of *Taylor and Stowe* [1984a, b] especially since their values were averaged over visible wavelengths. This result suggests that the pattern at 0.9 μm approximately represents the average over the solar spectrum.

Since the BRDF varied only slightly as the Sun moved in azimuth relative to the prevailing wind direction, it may be adequate for ERBE to use a BRDF that depends only on three angles rather than four, at least in February when the sastrugi are diminished. This approximation may, however, lead to significant inaccuracy in October and November when the sastrugi are well developed.

Measurements of the effect of sastrugi on BRDF are continuing. Some additional results with the same instrumentation were presented by *Brandt et al.* [1991].

Conclusions

The present set of observed spectral albedos agrees well with radiative transfer models even at visible wavelengths, where the albedo is indeed as high as 0.98. We confirm the predictions of *Bohren and Barkstrom* [1974]. Their formula for visible wavelengths, $\alpha_\lambda = 1 - 6[k_\lambda d]^{1/2}$, gives values in the range 0.98-0.96, where k_λ is the absorption coefficient for pure ice and d is the snow grain diameter. Our results also confirm the high visible albedos measured by *Liljequist* [1956] but do not agree with the low measured values of *Kuhn and Siogas* [1978].

On the basis of observations made under diffuse illumination, spectral albedo values measured at Vostok Station are essentially the same as at South Pole. Soot levels on the Antarctic plateau away from stations are low enough that they do not affect the spectral albedo of the snow. Thus we conclude that the vertical profile of near-surface grain size is sufficient to predict α_λ using radiative transfer theory. Photographs of surface snow grains on future Antarctic traverses would be useful in assessing the variability of albedo across the interior of the continent.

Acknowledgments. We are grateful for the logistics support provided by the National Science Foundation and the personnel at both McMurdo and Amundsen-Scott Stations. John Lynch, Cliff Wilson, and Brad Halter provided helpful discussion and technical assistance at South Pole Station. We also sincerely appreciate the support of Evgeniy Kononov, Station Leader at Vostok, and of the personnel of the 35th Soviet Antarctic Expedition, especially Aleksey Markov, who provided transportation by snowmobile to the remote sites for snow sampling. We thank Antony Clarke for considerable assistance with the soot measurements. We acknowledge Michael Kuhn, Gerd Wendler, and John Kelley for helpful discussions about their albedo measurements. Thanks also to Susan Marshall for measuring the snow grain sizes in our photographs and to Ellsworth Dutton for providing the daily albedos from NOAA's instruments at South Pole. Jennifer Francis, Richard Brandt, Craig Bohren and Petr Chýlek made many helpful comments on the manuscript. This work was supported primarily by the National Science Foundation under grants DPP-83-16220, DPP-88-18570, and DPP-91-20380. Additional support for equipment modification and maintenance was provided by the Office of Naval Research under grants N00014-90-J-1075 and N00014-89-J-1140.

References

Bohren, C. F., Applicability of effective-medium theories to problems of scattering and absorption by nonhomogeneous atmospheric particles, *J. Atmos. Sci., 43*, 468-475, 1986.

Bohren, C. F., Multiple scattering of light and some of its observable consequences, *Am. J. Phys., 55*, 524-533, 1987.

Bohren, C. F., and B. R. Barkstrom, Theory of the optical properties of snow, *J. Geophys. Res., 79*, 4527-4535, 1974.

Brandt, R. E., and S. G. Warren, Solar-heating rates and temperature profiles in Antarctic snow and ice, *J. Glaciol., 39*, 99-110, 1993.

Brandt, R. E., T. C. Grenfell, and S. G. Warren, Optical properties of snow, *Antarct. J. US, 26*, 272-275 , 1991.

Carlson, R. W., T. Arakelian, and W. D. Smythe, Spectral reflectance of Antarctic snow: "Ground truth" and spacecraft measurements, *Antarct. J. US, 27*, 296-298, 1992.

Carroll, J. J., Long-term means and short-term variability of the surface energy balance components at the south pole, *J. Geophys. Res., 87*, 4277-4286, 1982.

Carroll, J. J., and B. W. Fitch, Dependence of snow albedos on solar elevation and cloudiness at the south pole, *J. Geophys. Res., 86*, 5271-5276, 1981.

Chýlek, P., V. Ramaswamy, and V. Srivastava, Albedo of soot-contaminated snow, *J. Geophys. Res., 88*, 10,837-10,843, 1983.

Clarke, A. D., K. J. Noone, J. Heintzenberg, S. G. Warren, and D. S. Covert, Aerosol light absorption measurement techniques: Analysis and intercomparisons, *Atmos. Environ., 21*, 1455-1465, 1987.

Dutton, E. G., and J. R. Christy, Solar radiative forcing at selected locations and evidence for global lower tropospheric cooling following the eruptions of El Chichon and Pinatubo, *Geophys. Res. Lett., 19*, 2313-2316, 1992.

Dutton, E. G., R. S. Stone, and J. J. DeLuisi, South pole surface radiation balance measurements, April 1986 to February 1988, *NOAA Data Rep. ERL-ARL-17*, Natl. Oceanic and Atmos. Adm., Washington, D. C., 1989. (Available from NOAA Air Resources Laboratory, Silver Spring, Maryland.)

Gow, A. J., On the accumulation and seasonal stratification of snow at the South Pole, *J. Glaciol., 5*, 467-477, 1965.

Grenfell, T. C., A visible and near-infrared scanning photometer for field measurements of spectral albedo and irradiance under polar conditions, *J. Glaciol., 27*, 476-481, 1981.

Grenfell, T. C., A radiative transfer model for sea ice with vertical structure variations, *J. Geophys. Res., 96*, 16,991-17,001, 1992.

Grenfell, T. C., and G. A. Maykut, The optical properties of ice and snow in the Arctic Basin, *J. Glaciol., 18*, 445-463, 1977.

Grenfell, T. C., and D. K. Perovich, Radiation absorption coefficients of polycrystalline ice from 400 to 1400 nm, *J. Geophys. Res., 86*, 7447-7450, 1981.

Grenfell, T. C., and D. K. Perovich, Spectral albedos of sea ice and incident solar irradiance in the southern Beaufort Sea, *J. Geophys. Res., 89*, 3573-3580, 1984.

Grenfell, T. C., D. K. Perovich, and J. A. Ogren, Spectral albedos of an alpine snowpack, *Cold Regions Sci. Technol., 4*, 121-127, 1981.

Hansen, J. E., and L. D. Travis, Light scattering in planetary atmospheres, *Space Sci. Rev., 16*, 527-610, 1974.

Hanson, K., Radiation measurements on the Antarctic snowfield: a preliminary report, *J. Geophys. Res., 65*, 935-946, 1960.

Hoinkes, H. C., Studies of solar radiation and albedo in the Antarctic, *Arch. Meteorol. Geophys. Bioklimatol., B10*, 175-181, 1961.

Joseph, J. H., W. J. Wiscombe, and J.A. Weinman, The delta-Eddington approximation for radiative flux transfer, *J. Atmos. Sci., 33*, 2452-2459, 1976.

Kikuchi, K., and A. W. Hogan, Properties of diamond dust type ice crystals observed in summer season at Amundsen-Scott South Pole Station, Antarctica, *J. Meteorol. Soc. Jpn., 57*, 180-190, 1979.

Kou, L., D. Labrie, and P. Chýlek, Refractive indices of water and ice in the 0.65- to 2.5-μm spectral range, *Appl. Opt., 32*, 3531-3540, 1993.

Kuhn, M., Anisotropic reflection from sastrugi fields, *Antarct. J. US, 9*, 123-125, 1974.

Kuhn, M., Bidirectional reflectance of polar and alpine snow surfaces, *Ann. Glaciol., 6*, 164-167, 1985.

Kuhn, M., and L. Siogas, Spectroscopic studies at McMurdo, South Pole, and Siple Stations during the austral summer 1977-78, *Antarct. J. US, 13*, 178-179, 1978.

Kuhn, M., L. S. Kundla, and L. A. Stroschein, The radiation budget at Plateau Station, Antarctica, 1966-1967, *Antarct. Res. Ser., 25*, 41-73, 1977.

LaChapelle, E. R., ***Field Guide to Snow Crystals***, University of Washington Press, Seattle, 1969.

Li, S., ***A Model for the Anisotropic Reflectance of Pure Snow*** M.S. thesis, 60 pp., Univ. of Calif., Santa Barbara, , 1982.

Liljequist, G. H., Energy exchange of an Antarctic snow field: Short-wave radiation (Maudheim 71°03'S, 10°56'W), in ***Norwegian-British-Swedish Antarctic Expedition, 1949-52, Scientific Results***, vol. 2, part 1A, Norsk Polarinstitutt, Oslo, 1956.

McCartney, E. J., *Optics of the Atmosphere*, John Wiley, New York, 1976.

Perovich, D. K., and J. W. Govoni, Absorption coefficients of ice from 250 to 400 nm, *Geophys. Res. Lett., 18*, 1233-1235, 1991.

Peterson, J. T., *Geophysical Monitoring for Climate Change*, 145 pp., summary report 1977, U.S. Department of Commerce, Boulder, Co., 1978.

Rusin, N. P., Meteorological and Radiational Regime of Antarctica (in Russian), Gidrometeorologicheskoye Izdatel'stvo, Leningrad, 1961. (English translation, Israel Program for Scientific Translations, Jerusalem, 1964.)

Schlatter, T. W., The local surface energy balance and subsurface temperature regime in Antarctica, *J. Appl. Meteorol., 11*, 1048-1062, 1972.

Schwerdtfeger, W., ***Weather and Climate of the Antarctic***, Elsevier, New York, 1984.

Seckmeyer, G., and G. Bernhard, Cosine error correction of spectral UV-irradiances, *SPIE Proc., 2049*, 140-151, 1993.

Steffen, K., Bidirectional reflectance of snow at 500-600 nm, in ***Large Scale Effects of Seasonal Snow Cover***, edited by B. Goodison et al., *IAHS Publ. 166* pp. 415-425, Int. Assoc. of Hydrol. Sci., Wallingford, England, 1987.

Stephenson, P. J., Some considerations of snow metamorphism in the Antarctic ice sheet in the light of ice crystal studies, in ***Physics of Snow and Ice***, edited by H. Oura, pp. 725-740, Bunyeido, Sapporo, Japan, 1967.

Takano, Y., and K.-N. Liou, Solar radiative transfer in cirrus clouds, I, Single-scattering and optical properties of hexagonal ice crystals, *J. Atmos. Sci., 46*, 3-19, 1989.

Taylor, V. R., and L. L. Stowe, Reflectance characteristics of uniform Earth and cloud surfaces derived from Nimbus 7 ERBE, *J. Geophys. Res., 89*, 4987-4996, 1984a.

Taylor, V. R., and L. L. Stowe, Atlas of reflectance patterns for uniform Earth and cloud surfaces (Nimbus 7 ERB—61 days), *NOAA Techn. Rep. NESDIS 10*, Natl. Oceanic and Atmos. Adm., Washington, D. C., 1984b.

Warren, S. G., Optical properties of snow, *Rev. Geophys., 20*, 67-89, 1982.

Warren, S. G., Optical constants of ice from the ultraviolet to the microwave, *Appl. Opt., 23*, 1206-1225, 1984.

Warren, S. G., and A. D. Clarke, Soot in the atmosphere and snow surface of Antarctica, *J. Geophys. Res., 95*, 1811-1816, 1990.

Warren, S. G., and W. J. Wiscombe, A model for the spectral albedo of snow, II, Snow containing atmospheric aerosols, *J. Atmos. Sci., 37*, 2734-2745, 1980.

Warren, S. G., T. C. Grenfell, and P. C. Mullen, Optical properties of Antarctic snow, *Antarct. J. US, 21*, 247-248, 1986.

Wendler, G., and J. Kelley, On the albedo of snow in Antarctica: Contribution to I.A.G.O., *J. Glaciol., 34*, 19-25, 1988.

Wiscombe, W. J., Mie scattering calculations: Advances in technique and fast, vector-speed computer codes, *Tech. Note. NCAR/TN-140+STR (NTIS PB 301388)*, Natl. Cent. for Atmos. Res., Boulder, Colo., 1979.

Wiscombe, W. J., Improved Mie scattering algorithms, *Appl. Opt., 19*, 1505-1509, 1980.

Wiscombe, W. J., and S. G. Warren, A model for the spectral albedo of snow, I, Pure snow, *J. Atmos. Sci., 37*, 2712-2733, 1980a.

Wiscombe, W. J., and S. G. Warren, Solar and infrared radiation calculations for the Antarctic Plateau using a spectrally detailed snow reflectance model, in *International Radiation Symposium Volume of Extended Abstracts*, pp. 380-382, Colorado State University, Fort Collins, 1980b.

Wiscombe, W. J., R. M. Welch, and W. D. Hall, The effects of very large drops on cloud absorption, 1, Parcel models, *J. Atmos. Sci., 41*, 1336-1355, 1984.

Yamanouchi, T., Variations of incident solar flux and snow albedo on the solar zenith angle and cloud cover at Mizuho Station, Antarctica. *J. Meteorol. Soc. Jpn., 161*, 879-892, 1983.

T. C. Grenfell and S. G. Warren, Department of Atmospheric Sciences, AK-40, University of Washington, Seattle, WA 98195.

P. C. Mullen, Shapeware Corporation, 1601 5th Avenue, Suite 800, Seattle, WA 98101.

(Received October 12, 1993; revised May 24, 1994;
accepted June 2, 1994.)